The current issue and full text archive of this journal is available at
www.emeraldinsight.com/0961-5539.htm

Numerical simulation of turbulent flow in an industrial helical static mixer

Ramin K. Rahmani
Department of Mechanical Engineering, University of Alabama at Birmingham, Birmingham, Alabama, USA
Theo G. Keith
Department of Mechanical, Industrial and Manufacturing Engineering, The University of Toledo, Toledo, Ohio, USA, and
Anahita Ayasoufi
Department of Mechanical Engineering, University of Alabama at Birmingham, Birmingham, Alabama, USA

Received 4 September 2006
Revised 4 October 2007
Accepted 4 October 2007

Abstract

Purpose – Fluid mixing plays a critical role in the success or failure of industrial processes which call for the addition of small quantities of chemicals to working fluid. This paper aims to describe how mixing processes of liquids in turbulent flow regime can be simulated numerically, present the flow pattern through a helical static mixer, and provide useful information that can be extracted from the simulation results.

Design/methodology/approach – The performance of a helical static mixer under turbulent flow conditions is numerically studied. The model solves the 3D Reynolds-averaged Navier-Stokes equations, closed with the Spalart-Allmaras turbulence model, using a second-order-accurate finite-volume numerical method. Numerical simulations are carried out for a six-element mixer. Using a variety of predictive tools, mixing results are obtained and the performance of static mixer under turbulent flow condition is studied.

Findings – The upstream mixing elements increase the mixing more effectively compared to the downstream mixing elements; and also, the rate of mixing is higher in the regions close to the edges of mixing elements.

Practical implications – Static mixers have been widely used in the following industries: chemicals, food processing, heating, ventilation, and air conditioning, mineral processing, paints and resins, petrochemicals and refining, pharmaceuticals, polymers and plastics, pulp and paper, and water and waste treatment.

Originality/value – This paper fulfils an identified information need and offers practical help to an individual researcher in academia as well as industry.

Keywords Turbulent flow, Mixtures, Simulation, Chemicals

Paper type Research paper

Nomenclature

c_i	= concentration of traced particles ($i = 1, \ldots, N_s$)	$\bar{c}$	= averaged concentration
		d	= pipe diameter

This research was sponsored by Illinois Tool Works, Inc.

International Journal of Numerical Methods for Heat & Fluid Flow
Vol. 18 No. 6, 2008
pp. 675-696

0961-5539
DOI 10.1108/09615530810885515

$\mathbf{F}_i$ = external force vector ($i = 1, 2, 3$)
g = acceleration due to gravity
I = turbulence intensity
k = turbulence kinetic energy
n = power law index
N_s = total number of plane sectors
$N_{(i)}$ = number of particles placed in the ith sector in the flowfield cross-section (to determine PDU)
N_l = number of symmetry lines that the flowfield cross-section is divided into (to determine PDU)
$N_{Left}(i)$ = number of particles on the left side of the ith symmetry line
$N_{Right}(i)$ = number of particles on the right side of the ith symmetry line
p = pressure
Re = Reynolds number ($= \rho U d/\mu$)
Re_{D_H} = Reynolds number based on the hydraulic diameter
r_s = structure radius
t^* = non-dimensionalized residence time
U = bulk velocity
V_m = mixer volume
$\mathbf{u}_i$ = velocity vector ($i = 1, 2, 3$)
$\mathbf{x}_i$ = position vector ($i = 1, 2, 3$)
δ_{ij} = Kroncker delta ($= 1$ if $i = j$, $= 0$ if $i \neq j$)
ϵ = turbulence energy dissipation
μ = molecular viscosity
ρ = density
$-\rho\overline{\mathbf{u}'_i\mathbf{u}'_j}$ = Reynolds stresses ($i, j = 1, 2, 3$)
τ_{ij} = stress tensor ($i, j = 1, 2, 3$)
ω = specific dissipation

Introduction

Mixing is an essential component of nearly all industrial chemical processes, ranging from simple blending to complex multi-phase reaction systems for which reaction rate, yield and selectivity are highly dependent upon mixing performance. Consequences of improper mixing include non-reproducible processing conditions and lowered product quality, resulting in the need for more elaborate downstream purification processes and increased waste disposal costs.

The static mixer has increased in popularity within industry over recent years. They have been widely used in the following industries: chemicals, food processing, heating, ventilation, and air conditioning, mineral processing, paints and resins, petrochemicals and refining, pharmaceuticals, polymers and plastics, pulp and paper, and water and waste treatment. Typical fluid varies from low-viscosity gases to highly viscous non-Newtonian liquids. Generally, a static mixer consists of a number of equal stationary units placed on the inside of a pipe or channel in order to promote mixing of flowing fluid streams. These mixers have low maintenance and operating costs, low-space requirements and no moving parts. One of the most common static mixers is the helical static mixer. A helical static mixer consists of left- and right-twisting helical elements placed at an angle of 90° to each other. In a standard mixer, each element twists through an angle of 180°. The complete mixer unit is a series of elements arranged axially within a pipe so that the leading edge of each element is at right angles to the trailing edge of the previous element (Figure 1). The range of practical Reynolds numbers for helical static mixers in industrial applications is usually from very small to moderate values; however, it has been found that the flow regime in helical static mixers is turbulent for relatively low Reynolds numbers, compared to flow inside a pipe with no mixing elements present. Some other static mixers that are used in turbulent flow regimes are: Inliner, Komax, LPD, and SMV.

The use of CFD to obtain the velocity field in some commercial mixers has been a research topic over the past 15 years (Khakhar *et al.*, 1987; Kusch and Ottino, 1992; Hobbs and Muzzio, 1998; Jones *et al.*, 2002; Byrde and Sawley, 1999a, b). The majority

of the previous work has focused on model flows that are 2D and time periodic; and a smaller set of studies have considered 3D, spatially periodic flows (Khakhar *et al.*, 1987; Kusch and Ottino, 1992) where a simplified, 2D analytical approximation to the velocity field was obtained. Also, in spite of this fact that a wide range of mixing processes occur in the turbulent flow regime, most of the previous work has focused on laminar flows.

The $k - \omega$ model has been validated (Jones, 1999) and used to study the flowfield across helical static mixers (Jones *et al.*, 2002; Rahmani *et al.*, 2005, 2006a). In this paper, first it is shown that Spalart-Allmaras model is able to produce the same results as the $k - \omega$ model, in order to simulate the flow in an industrial helical static mixer, while it is computationally much less expensive. Then it is used to study the global performance of the mixer. In the following sections, first the governing equations and the turbulence model are described briefly. The numerical method is explained next, followed by description of key parameters used to evaluate a mixer performance. The obtained results and discussion are presented after a brief part on the accuracy of the numerical study. The geometrical parameters of the mixer studied here are provided in Table I.

Analysis

Governing equations

For steady incompressible flow, the conservation of mass and the conservation of momentum equations can be written as:

$$\frac{\partial \mathbf{u}_i}{\partial \mathbf{x}_i} = 0 \tag{1}$$

$$\rho \frac{\partial (\mathbf{u}_i \mathbf{u}_j)}{\partial \mathbf{x}_j} + \frac{\partial p}{\partial \mathbf{x}_i} = \frac{\partial \tau_{ij}}{\partial \mathbf{x}_j} + \rho g_i + \mathbf{F}_i \tag{2}$$

In the absence of a gravitational body force and any external body forces, the two last terms on the right side of equation (2) are zero. The stress tensor τ_{ij} in equation (2) is given by:

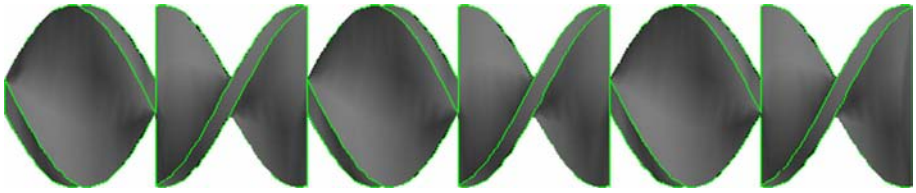

Figure 1.
A six-element static mixer

Diameter (d)	4.80 mm
Segment (element) length	4.06 mm
Thickness	0.89 mm
Entrance length	9.60 mm
Exit length	9.60 mm

Table I.
Typical static mixer dimensions

$$\tau_{ij} = \mu\left(\frac{\partial \mathbf{u}_i}{\partial \mathbf{x}_j} + \frac{\partial \mathbf{u}_j}{\partial \mathbf{x}_i}\right) - \frac{2}{3}\mu\frac{\partial \mathbf{u}_k}{\partial \mathbf{x}_k}\,\delta_{ij} \tag{3}$$

For incompressible steady flows, the last term of equation (3) is zero.

Turbulence modeling

Turbulent flows are characterized by fluctuating velocity fields. These fluctuations mix transported quantities of mass, momentum, and energy and in turn cause the transported quantities to fluctuate as well. Since a complete time-dependent solution of the exact Navier-Stokes equations for turbulent flows in complex geometries is too expensive, two alternative methods have been employed to transform the Navier-Stokes equations in such a way that the small-scale turbulent fluctuations do not have to be directly simulated: Reynolds averaging and filtering. However, both methods introduce additional terms in the governing equations that need to be modeled.

The Reynolds-averaged Navier-Stokes (RANS) equations represent transport equations for the mean flow quantities; and all the scales of the turbulence are modeled. This approach significantly reduces the computational effort; and therefore, the use of RANS models is preferred for practical engineering calculations.

In this study, the 3D, steady RANS equations are solved. The momentum equation can be written as:

$$\rho\frac{\partial(\mathbf{u}_i\mathbf{u}_j)}{\partial \mathbf{x}_j} = \frac{\partial}{\partial \mathbf{x}_j}\left[\mu\left(\frac{\partial \mathbf{u}_i}{\partial \mathbf{x}_j} + \frac{\partial \mathbf{u}_j}{\partial \mathbf{x}_i}\right) - \frac{2}{3}\mu\frac{\partial \mathbf{u}_k}{\partial \mathbf{x}_k}\,\delta_{ij}\right] - \frac{\partial p}{\partial \mathbf{x}_i} + \frac{\partial}{\partial \mathbf{x}_j}\left(-\rho\overline{\mathbf{u}'_i\mathbf{u}'_j}\right) \tag{4}$$

Considering the conservation of mass for an incompressible steady flow, $(\partial \mathbf{u}_k/\partial \mathbf{x}_k) = 0$, in equation (4).

The Reynolds stresses, $-\rho\overline{\mathbf{u}'_i\mathbf{u}'_j}$, must be modeled in order to close the set of equations. In 1877, Boussinesq introduced the concept of an eddy viscosity. As with Reynolds, Boussinesq has been immortalized in turbulence literature. In turbulence models that employ the Boussinesq approach, the central issue is how the eddy viscosity is computed.

Based on the Boussinesq hypothesis, Kolmogorov (1942) introduced the first complete model of turbulence. In addition to having a modeled equation for the kinetic energy of the turbulent fluctuations, k (Prandtl, 1945), Kolmogorov introduced a second parameter ω that he referred to as the rate of dissipation of energy per unit volume and time. The reciprocal of ω serves as a turbulence time scale, while $\sqrt{k}/\omega$ serves as the analog of the mixing length. The $k - \omega$ model has been validated extensively in complex, 3D shear flows (Sotiropoulos and Ventikos, 1998; Lin and Sotiropoulos, 1997). The $k - \omega$ model introduced by Menter (1994), which is a modified version of the original model of Wilcox (1988) has been used to study turbulent flow across helical static mixers (Jones, 1999; Rahmani *et al.*, 2006a).

The model proposed by Spalart and Allmaras (1992) solves a transport equation for a quantity that is a modified form of the turbulent kinematic viscosity. In these models a transport equation is solved for a turbulent quantity (usually the turbulent kinetic energy) and a second turbulent quantity (usually a turbulent length scale) is obtained from an algebraic expression. The turbulent viscosity is calculated from

the Boussinesq assumption. This model is incomplete however as it relates the turbulence length scale to some typical flow dimension.

The Spalart-Allmaras model is a relatively simple one-equation model that solves a modeled transport equation for the kinematic eddy viscosity. This embodies a relatively new class of one-equation models in which it is not necessary to calculate a length scale related to the local shear layer thickness. The Spalart-Allmaras model was designed specifically for aerospace applications involving wall-bounded flows and has been shown to give good results for boundary layers subjected to adverse pressure gradients. It is also gaining popularity in turbomachinery applications, e.g. as described by Nürnberger and Greza (2002). This model is effectively a low-Reynolds number model, requiring the viscous-affected region of the boundary layer to be properly resolved.

It should be mentioned that using the Spalart-Allmaras model, the near-wall gradients of the transported variable in this model are much smaller than the gradients of the transported variables in the $k - \epsilon$ (Launder and Spalding, 1972) and $k - \omega$ models. This might make the model less sensitive to numerical error when non-layered meshes are used near walls. The original model is based on the idea that, for the wall-bounded flows that were of most interest when the model was formulated, turbulence is found only where vorticity is generated near walls. However, it has since been acknowledged that one should also take into account the effect of mean strain on the turbulence production, and a modification to the model has been proposed by Dacles-Mariani *et al.* (1995), which combines measures of both rotation and strain tensors. In fact, Dacles-Mariani *et al.*, introduced a modification to the Baldwin and Barth (1990) turbulence model, which is based on the idea previously proposed by Spalart (Spalart and Allmaras, 1992; Dacles-Mariani *et al.*, 1995). Including both the rotation and strain tensors reduces the production of eddy viscosity and consequently reduces the eddy viscosity itself in regions where the measure of vorticity exceeds that of strain rate. One such example can be found in vortical flows, i.e. flow near the core of a vortex subjected to a pure rotation where turbulence is known to be suppressed. Including both the rotation and strain tensors more correctly accounts for the effects of rotation on turbulence. The default option (including the rotation tensor only) tends to over-predict the production of eddy viscosity and hence over-predicts the eddy viscosity itself in certain circumstances.

Numerical method

The numerical simulation of the flow and mixing in a helical static mixer has been performed via a two-step procedure. In the first step, the flow velocity (and the pressure) is computed. The velocity values are then used as input to the second step that consists of the calculation of trajectories of particles (here, fluid elements) within the computed flow field.

The solver used in this study for the flow field computation (the first step) is a commercial code: FLUENT, version 6.0 (a registered trademark of Fluent Inc., a wholly owned subsidiary of ANSYS, Canonsburg, PA, USA). The selected solver uses segregated, implicit, and second-order upwind (Warming and Beam, 1975) method. Pressure-velocity coupling is achieved by using the SIMPLEC (SIMPLE-Consistent) algorithm (Vandoormaal and Raithby, 1984). All calculations were performed in double precision.

No-slip boundary conditions are applied to the solid surface of the static mixer and also at the wall of the pipe. A constant mass flow rate is applied at the inlet and outlet boundaries. Fully developed flow conditions are assumed at the inlet; the one seventh-root law is used for the velocity profile at the flow field inlet. The turbulence intensity is used to specify the turbulent boundary conditions at the flow inlet. The turbulence intensity (the root-mean-square of the streamwise velocity fluctuations normalized by the mean flow velocity) for a fully-developed duct flow can be estimated, using the following empirical correlation for pipe flows:

$$I = 0.16\left(Re_{D_{\mathrm{H}}}\right)^{-(1/8)} \tag{5}$$

The turbulence intensity, for the geometry used here, is equal to 6.99 percent for the case of $Re = 3{,}000$.

The second step of the computation process is to track the fluid particles. To determine the efficiency of a mixer, it is necessary to establish a means by which the fluid mixing can be gauged both qualitatively and quantitatively. Here, this was achieved by calculating the trajectories of fluid elements in the flow field of the mixer.

For a steady laminar flow, fluid particle trajectories correspond to streamlines. Therefore, for those cases, trajectories can be tracked by integrating the vector equation of motion, using the numerically computed velocity field as input, i.e.:

$$\frac{\mathrm{d}\mathbf{x}_i}{\mathrm{d}t} = \mathbf{u}_i \tag{6}$$

However, for turbulent flows, some considerations in using the results of a steady RANS calculation are needed. In turbulent flows scalar transport and stirring is the result of both by the large-scale coherent vortices and the broad range of turbulent eddies. RANS modeling procedure smoothes flowfield and therefore, particle tracking using the statistically stationary mean flow as the advecting velocity field does not take into account the effect of small scale turbulence on transport. In order to overcome this shortcoming, turbulent Reynolds stresses can be used to generate instantaneous velocity. In RANS turbulence modeling approach, information about turbulent fluctuations is contained in the time averaged Reynolds stresses of the form $\overline{\mathbf{u}'_i\mathbf{u}'_j}$. Stochastic techniques can be used in order to generate a random fluctuating velocity field using the turbulence intensities. These fluctuations are superimposed to the calculated time-averaged velocity field and create an instantaneous velocity fields. Fluid particle tracking is carried out using this instantaneous flowfield (Rahmani *et al.*, 2005).

Some care must be taken in integrating the particle motion equation in order to retain a sufficient degree of accuracy. To obtain an accurate global evaluation of the mixing, the study of the trajectories of a large number of particles was undertaken.

Preliminary tests indicated that while lower order schemes appear to provide acceptable results, they accentuate the problem of lost particles (particles that are trapped near a solid wall, where the local velocity is zero, or leave the computational domain). Hence, a fourth order Runge-Kutta integration algorithm with adaptive step-size control was employed. To avoid problems near stagnation points, the numerical integration of the streamline equation was performed using a fixed spatial increment rather than a fixed time step. By this method, the particle locations within

the cross-sections of the flow field can be obtained. With these considerations, the number of lost particles was minimized to not more than 7.29 percent. No attempt was made to recover lost particles by re-injection into the flow field, since this may unduly perturb the mixing analysis.

At the entry of the inlet pipe section, 501,740 zero-mass and zero-volume particles were distributed uniformly over half of the inlet surface. This can be viewed as a simplified model for the diametrical feeding of the mixer with two component fluids.

G-value

Camp and Stein (1943) developed the root-mean-squared *G*-value to quantify the mixing in turbulent flocculation basins by analogy with the shear rate in a simple, one-dimensional, laminar shear flow, the Couette flow. The *G*-value became a universal measure of mixing in the following decades. For any in-line mixer, the *G*-value is calculated based on the energy losses that occur in the mixer (Rahmani *et al.*, 2005). For the static mixer studied here:

$$G - \text{value} = \frac{1}{2}\left(\frac{\pi d}{V_{\text{m}}}\right)^{1/2}\left(\frac{Re\,\Delta p}{\rho}\right)^{1/2} \tag{7}$$

As can be seen from equation (7), for a given geometry and a specific Reynolds number, the *G*-value is a function of material density and the pressure drop of the flow in the mixer. It has been demonstrated that the original derivation of the *G*-value was flawed for 3D flows (Clark, 1985; Graber, 1994) and cannot be universally applied to different types of mixers or different size mixers. Nonetheless, the *G*-value remains entrenched in the engineering literature and continues to be used (Jones *et al.*, 2002). Because of that and also because it can be calculated easily, it is not entirely futile to use the obtained numerical results to calculate *G*-value and explore it.

Residence time distribution

The residence time distribution (RTD) is used to characterize the uniformity of the history of fluid elements in the static mixer. A similar history for all fluid elements in the flow is a desirable feature in order to provide the uniformity of the product quality. This can be achieved by a narrow distribution of the residence times for chemical reactors. RTD for flows in a static mixer has been studied experimentally (Tung, 1976) and numerically (Kemblowski and Pustelnik, 1988; Hobbs and Muzzio, 1997; Nauman, 1991). Here, the RTD for a flow in a helical static mixer was calculated by tracking about 266,000 uniformly spaced, zero-mass, zero-volume, particles initially located in the top half of the flow field inlet. The residence time of each particle was measured from the point when the particle passes the cross-sectional plane of the leading edge of the first mixing element to the point when the particle passes the cross-sectional plane of trailing edge of the last mixing element. The measured residence time is non-dimensionlized by the residence time of a fluid particle traveling at the bulk flow velocity in a pipe with no mixer. Given the value of the non-dimensionlized residence time (t^*) for all fluid particles which have passed the cross-sectional plane, the fraction of the volumetric flow, which has a residence time between t^* and $t^* + \mathrm{d}t^*$ can be calculated. This parameter is known as the distribution function, $f(t^*)$.

Structure radius

As a quantitative measure of the fluid mixing, the size of the structures at different flow cross-sections is considered. The 2D structure radius at a given axial location, r_s, normalized to the pipe radius, has been defined to correspond to the radius of the largest circle that can be drawn around a particle of one of the fluid components that does not contain any particles of the other fluid component (Byrde, 1997). This structure radius corresponds to the striation thickness generally measured experimentally (Byrde and Sawley, 1999b).

Intensity of segregation

The intensity of segregation is defined as the ratio of the variance of the concentration values over the variance of the segregated system (Danckwerts, 1952). The heterogeneity of the mixture can be represented in terms of the variance of such measurements, defined as:

$$s^2 = \frac{1}{N_s - 1} \sum_{i=1}^{N_s} (c_i - \bar{c})^2 \tag{8}$$

The normalization of the variance to its maximum value, $\bar{c}(1 - \bar{c})$, is called intensity of segregation. Intensity of segregation is a measure of the deviations of concentration within dissimilar regions of a mixture. It varies between zero and one. When the intensity of segregation is zero, an ideal distributive mixing is obtained. A value of one represents total segregation. In practice, however, the values of intensity of segregation, even for a very poor mixture, lie much closer to zero than to one (Onwulata, 2005).

The coefficient of variation (COV) can be used to measure the intensity of segregation (Rahmani *et al.*, 2006b):

$$\mathrm{COV} = \frac{1}{\bar{c}} \sqrt{\frac{\sum_{i=1}^{N_s} (c_i - \bar{c})^2}{N_s - 1}} \tag{9}$$

Particles distribution uniformity

Another suitable tool for measuring the degree of mixing quantitatively is the particles distribution uniformity (PDU), which is defined as (Rahmani *et al.*, 2005):

$$\mathrm{PDU} = \left(1 - \frac{1}{2(1 - (1/N_s))} \sum_{i=1}^{N_s \to \infty} pd_1(i)\right)\left(1 - \frac{1}{N_1} \sum_{i=1}^{N_1 \to \infty} pd_2(i)\right) \tag{10}$$

In equation (10) pd_1 and pd_2 are, respectively, called the particle distribution function of the first kind and of the second kind, which are given by:

$$pd_1(i) = \frac{|(N_p/N_s) - N_{(i)}|}{N_p} \tag{11}$$

$$pd_2(i) = \frac{|N_{\mathrm{Left}}(i) - N_{\mathrm{Right}}(i)|}{N_p} \tag{12}$$

PDU varies from zero to one. For perfect mixing situation, the PDU value is one, otherwise it is less than one. A low-PDU value indicates poor mixing in the

flow cross-section. It is mentioned that the computational time needed to determine the intensity of segregation is about two times the computational time which is needed to calculate the value of PDU for each case (Rahmani *et al.*, 2006b). Particle trajectories corresponding to only one of the fluids need to be calculated in order to determine PDU or RTD; however, in order to determine COV or structure radius, particle trajectories corresponding to both of the fluids are calculated.

Numerical solution accuracy

It is important that the accuracy of the numerical solutions be analyzed before confidence in the predictive ability of the numerical techniques can be justified. For the present study of mixing under non-creeping flow conditions, there is unfortunately an absence of experimental data that is sufficiently detailed and accurate to undertake a complete validation of the numerical results. However, comparison with existing experimental values of the pressure drop across the mixer measured shows very good agreement with the numerically determined values. In addition, a detailed mesh convergence study has indicated that the computational mesh employed in the present study is sufficiently refined to provide good numerical resolution. The computed pressure drop in the pipe containing the mixer is contrasted to the measured data. Also, the velocity contours at the computational flow field outlet are considered.

For the particle tracking studies, different numbers of particles (from 457 particles up to 1,225,784 particles) were used to analyze the mixing. By increasing the number of particles, it is possible to discern finer structures and thus quantify the mixing efficiency with higher precision (Rahmani *et al.*, 2005). It was observed that 501,740 particles at the flow inlet can give a correct image of mixing; although using a higher number of particles leads to a more pronounced mixing pattern, but the difference between the obtained results is not that significant to justify the computational cost needed for calculations.

Results and discussion

Applying the numerical method described above, the flow of an incompressible Newtonian fluid across a six-element static mixer has been analyzed using a 2.02 GHz AMD Athlon 64 $\times$ 2 processor. As for the convergence criterion, a scaled residual less than 10^{-5} for all scalar equations, is used here. Table II shows the values of pressure drop across the mixer, area-weighted average velocities, and area-weighted average vorticity at the end of the 6th mixing element, non-dimensionalized by the values as predicted from the converged solution, using the Spalart-Allmaras model. The results obtained were found to vary negligibly once this condition was reached.

Iterations	Pressure drop ratio	Averaged velocity ratio at the 6th element	Averaged vorticity ratio at the 6th element
4650	1.000551	1.000311	1.000451
4850	0.999891	1.000030	1.000054
5050	1.000019	1.000099	1.000312
5250	0.999998	0.999998	0.999971
5450	0.999999	1.000002	1.000002
5650	1.000000	1.000000	1.000000

Table II. Convergence of pressure drop across the mixer, averaged velocity, and averaged vorticity

An unstructured hexagonal mesh was generated to model the six-element static mixer inside a pipe, using a code developed by the authors (Rahmani *et al.*, 2005). Table III gives the information related to the computational grid used in this study for the Spalart-Allmaras and the $k - \omega$ turbulence models. Maximum y^+ is about 3 for both cases. The mesh size for the Spalart-Allmaras model is slightly coarser than the mesh size used by the $k - \omega$ model. Table IV presents a comparison of the number of iterations, the required CPU time per iteration and the computational memory needed for the $k - \omega$ and the Spalart-Allmaras turbulence models, using the same computational grid. The CPU time for each model is non-dimensionlized by the CPU time needed for one iteration using the $k - \omega$ model and the computational memory is also non-dimensionlized by the memory needed using the $k - \omega$ model. The total CPU time for the Spalart-Allmaras model is 0.70 times of the total CPU time using the $k - \omega$ model. Considering the fact that, in practice, the Spalart-Allmaras model needs a grid slightly coarser than the grid needed by the $k - \omega$ model, the Spalart-Allmaras model needs even less computational time and memory.

The velocity fields for both turbulence models were obtained. The cross-sectional velocity vectors are shown in Figures 2 and 3, which show the cross-sectional projection of the velocity vectors at the end of the 2nd, the 4th, and the 6th elements. Contours of velocity magnitude are shown in Figures 4 and 5. The velocity field predicted by the Spalart-Allmaras and $k - \omega$ models are quiet similar. The Spalart-Allmaras and $k - \omega$ models were designed for applications involving wall-bounded flows and low-Reynolds number regions. On the other hand, the standard $k - \epsilon$ model is designed for high-Reynolds turbulent flows. The $k - \epsilon$ and the RSM models are designed for turbulent flows in regions somewhat far from walls. Therefore, for the flow considered here, which is surrounded by solid walls and filled by low-Reynolds number regions, turbulence models that rely on wall treatments are not able to predict a very accurate and detailed velocity field.

The mean and the maximum vorticity magnitudes at these mixing elements are presented in Table V. A very small difference between the predictions of two models can be observed.

Determining the pressure drop across a static mixer is essential in order to correctly size the extruder or pump, feeding the mixer. The predicted pressure drop through the mixer by different models is shown in Table VI. The experimentally measured pressure drop through the mixer is 1,180 Pa. Both turbulence models are able to predict the pressure drop accurately.

Table III.
Mesh information for the turbulent flow cases

Model	Number of cells	Minimum $y+$	Maximum $y+$
Spalart-Allmaras	2,296,158	0.11	3.01
$k - \omega$	2,335,690	0.11	2.96

Table IV.
CPU time and memory used by different turbulence models

Model	Iterations	CPU time per iteration	Memory
Spalart-Allmaras	5,650	0.60	0.88
$k - \omega$	4,820	1.00	1.00

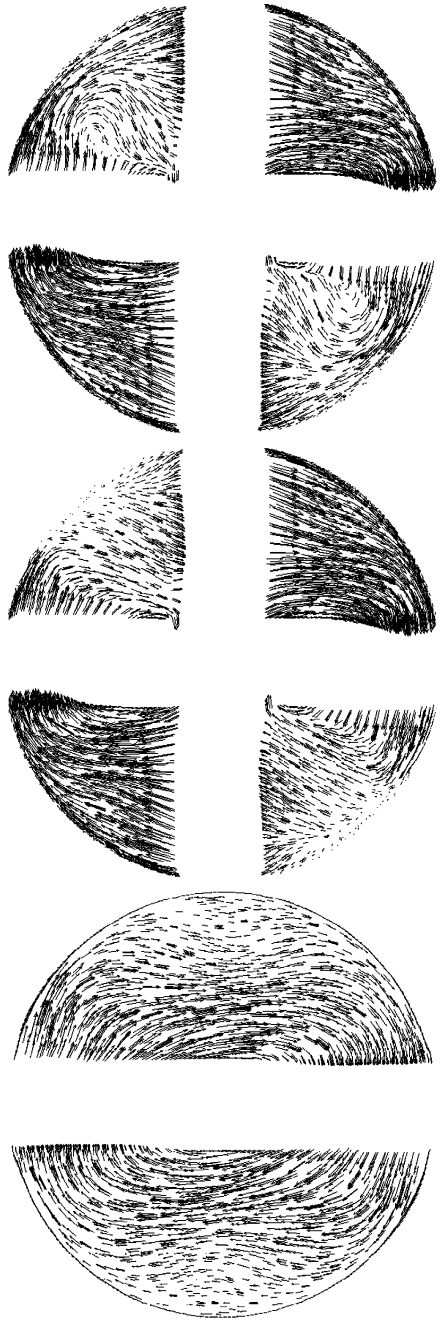

Note: Spalart-Allmaras model

Figure 2.
Velocity field, from top to bottom: at 2nd, 4th, and 6th mixing element

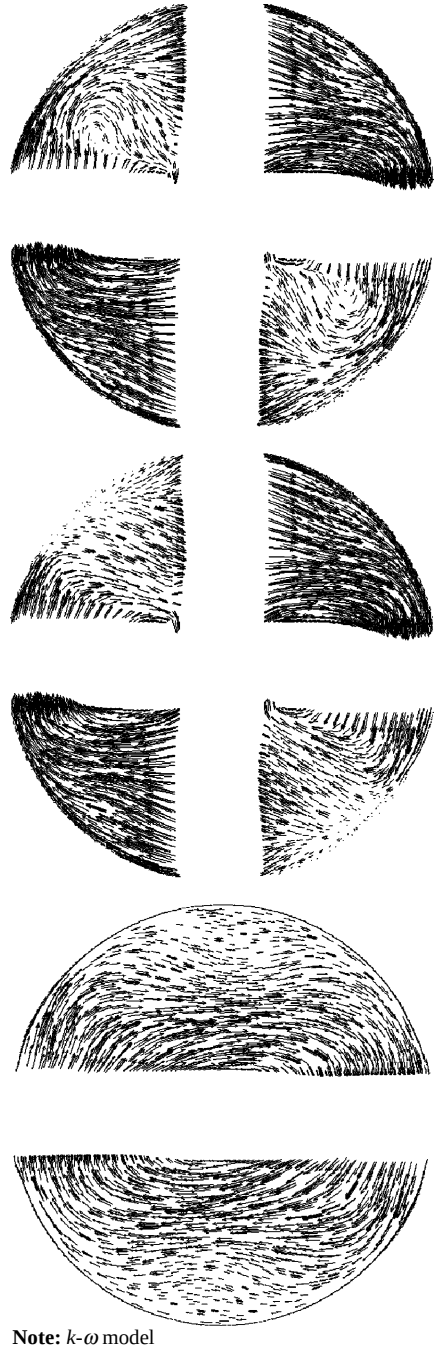

Note: k-ω model

Figure 3.
Velocity field, from top to bottom: at 2nd, 4th, and 6th mixing element

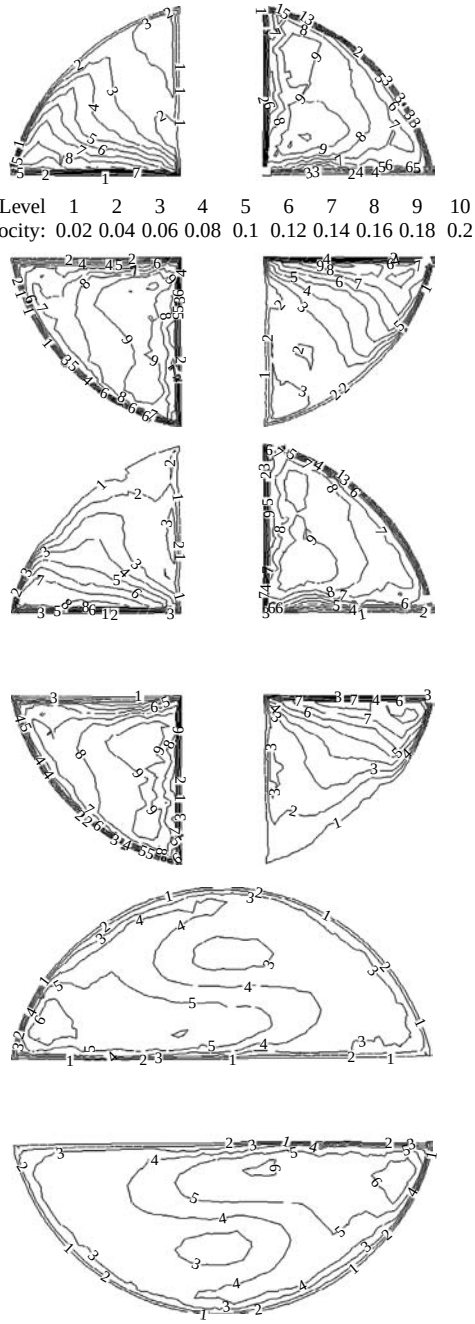

Note: Spalart-Allmaras model

Figure 4.
Velocity contours (m/s), from top to bottom: at 2nd, 4th, and 6th element

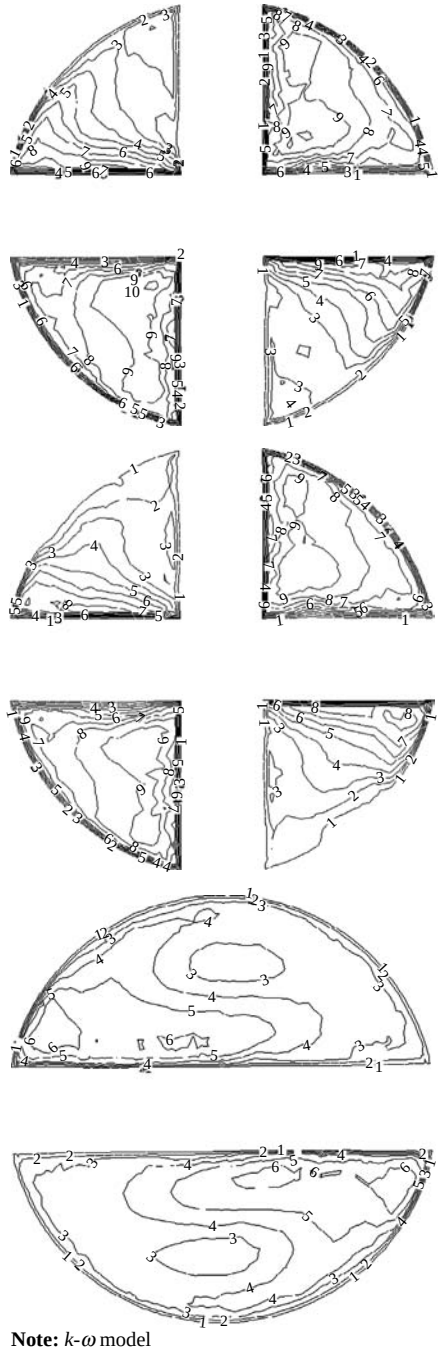

Note: k-ω model

Figure 5.
Velocity contours (m/s), from top to bottom: at 2nd, 4th, and 6th element

Figure 6 shows the distribution function for flow across a six-element helical static mixer inside a pipe. The non-dimensional time step, dt^*, is 0.01. Both models predict similar RTD. The maximum non-dimensionlized residence time, t^*, predicted by Spalart-Allmaras model is about 2.3. Non-dimensionlized residence time is from about $t^* = 0.5$ to about $t^* = 1.4$ for the majority of fluid elements. Table VII shows values of the standard deviation of the distribution function, based on the velocity domain predicted by different turbulent models. As can be seen, the value of standard deviation is very small, suggesting that a large portion of fluid elements experience

Model		Spalart-Allmaras	$k - \omega$
Mean vorticity 1/*s*	2nd	2,679.29	2,700.04
	4th	2,775.27	2,791.02
	6th	243.41	249.25
Maximum vorticity 1/*s*	2nd	2,0751.85	20,481.51
	4th	19,541.44	19,247.37
	6th	6,782.05	5,593.88

Table V.
Vorticity magnitude at 2nd, 4th, and 6th mixing element

Model	Pressure drop (Pa)
Spalart-Allmaras	1,161.43
$k - \omega$	1,167.41

Table VI.
Pressure drop predicted by different turbulence models

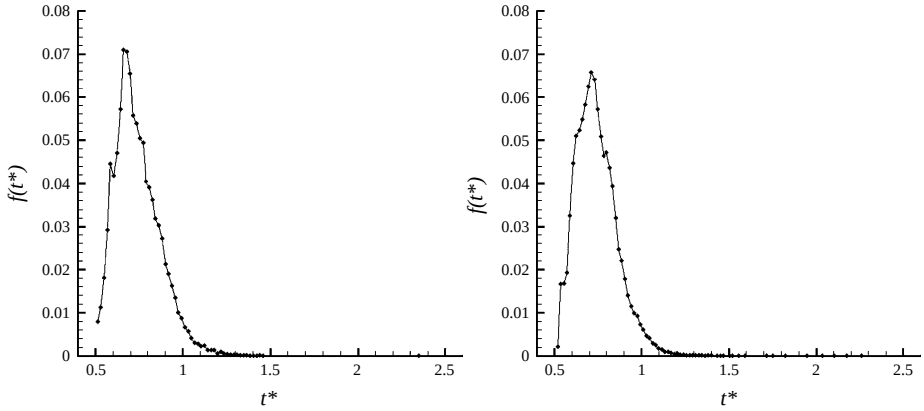

Note: Left: Spalart-Allmaras, Right: *k-ω*; Reproduced from the only available original

Figure 6.
Distribution function for flow in the six-element static mixer

Model	SD
Spalart-Allmaras	1.8663×10^{-2}
$k - \omega$	1.8726×10^{-2}

Table VII.
Standard deviation of distribution function

almost similar traveling time across the mixer. Also, it can be seen that both values predicted based on the two different turbulent models are almost the same.

The trajectories of the particles injected into the mixer from the top half on flow inlet have been calculated using the Spalart-Allmaras model. The impact of the relative location of each fluid component at inlet with respect to the leading edge of the first mixing element on the mixing is not significant, when the fluid passes the first few mixing elements (Rahmani *et al.*, 2006c). Figure 7 shows the redistribution of fluid elements in different cross-section of flow across the first mixing element. The ratio x/L in this figure represents the distance of the flow cross-section from the leading edge of the first element divided by the length of the mixing element. These plots illustrate the redistribution of the released particles via the combined effects of flow division and reversal, resulting in stretching and folding of the observed structures. Mixing element redistributes fluid elements more effectively at the areas near its edges.

The plots of the particle positions at the end of the 2nd, the 4th, and the 6th elements are shown, respectively, from left to right, in Figure 8. Comparing the results at different cross-sections (Figures 7 and 8) reveals that islands of separated fluid elements are distinguishable after the flow passes the first mixing element. These islands are divided into several small regions after the flow passes the fourth element; the level of darkness in the corresponding figures decreased, suggesting that two fluids are penetrating each other. After the 6th element, the large portion of field is filled with gray regions and the particles are distributed more uniformly in the mixer cross-section; the area of the flow cross-section containing no particles is much smaller.

The turbulence intensity in the flow inlet has a major impact on the particles trajectory and therefore on the mixing of the working fluids at the first few upstream mixing elements. It was observed, that as the flow passes through more mixing elements the distribution of the particles is less affected by the turbulence intensity at the flow inlet. Moreover, after the 6th mixing element this effect has almost vanished.

Values of the structure radius at the end of even numbered mixing elements are given in Table VIII. As expected, the structure radius decreases as the flow passes through the static mixer. The rate of change of the structure radius from the flow cross-section at the end of the 2nd element to the end of the 4th element is higher than the one from the flow cross-section at the end of the 4th element to the end of the 6th element. This suggests that, the upstream mixing elements increase the mixing more efficiently compared to the downstream mixing elements.

Predicted values for intensity of segregation and the rate of its changes with respect to the axis of the mixer are shown in Figures 9 and 10. The dashed-lines in the figures show the axial location of the leading and/or trailing edge of each mixing element. Although the value of intensity of segregation oscillates, overall it decreases as the flow passes through the mixer. Local maximums can be observed close the trailing edge of each element, followed by a sharp decrease in the value of intensity of segregation after flow passes the leading edge of each element. The first mixing element does not improve mixing significantly; however, overall the first few upstream mixing elements (specially the second element) manifest higher impact on the fluid mixing compared to the others. The impact of the first element on the mixing can be improved if the relative position of the two fluid components to the leading edge of the first element is in a way that each fluid component is divided into almost half by the leading edge. Creating such an ideal situation in practice might not be straightforward.

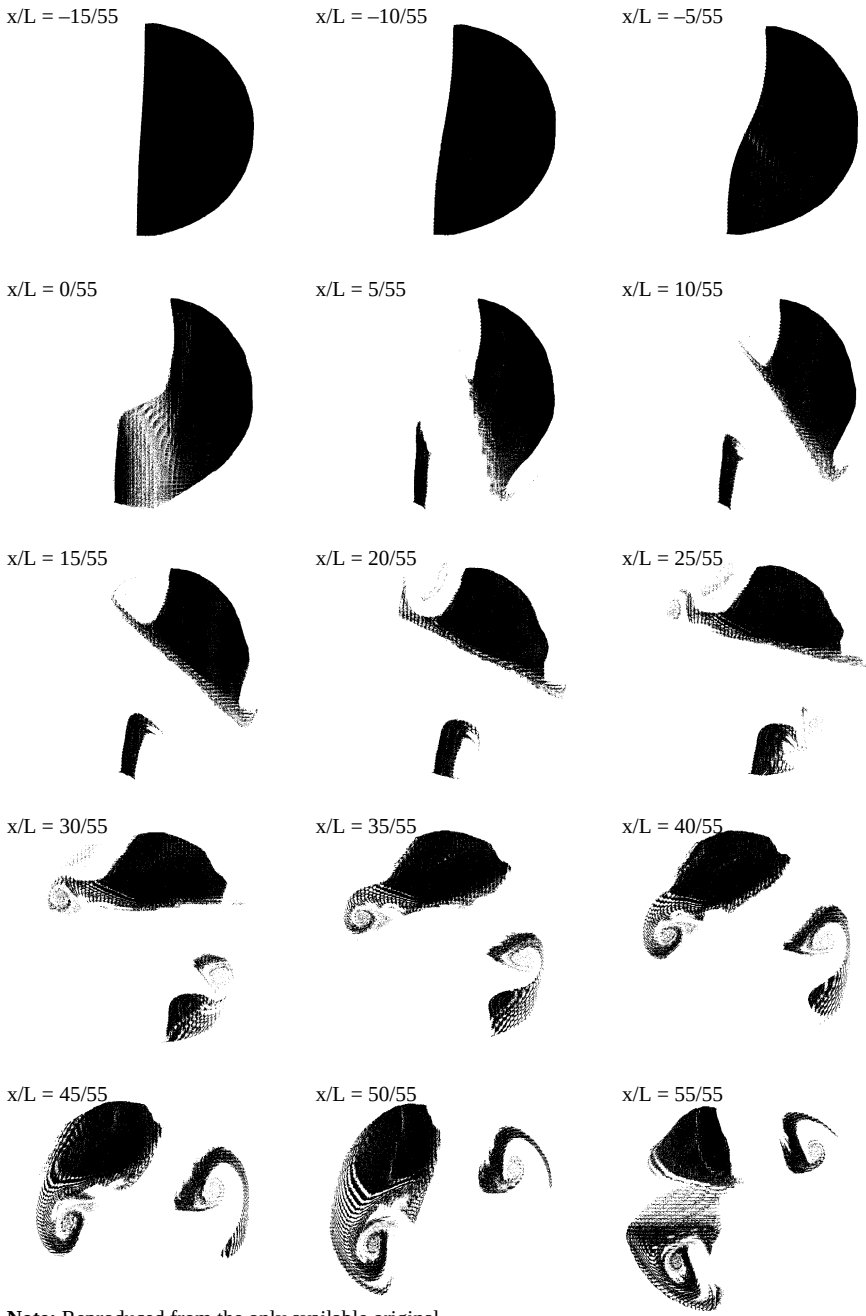

Note: Reproduced from the only available original

Figure 7.
Distribution of fluid particles

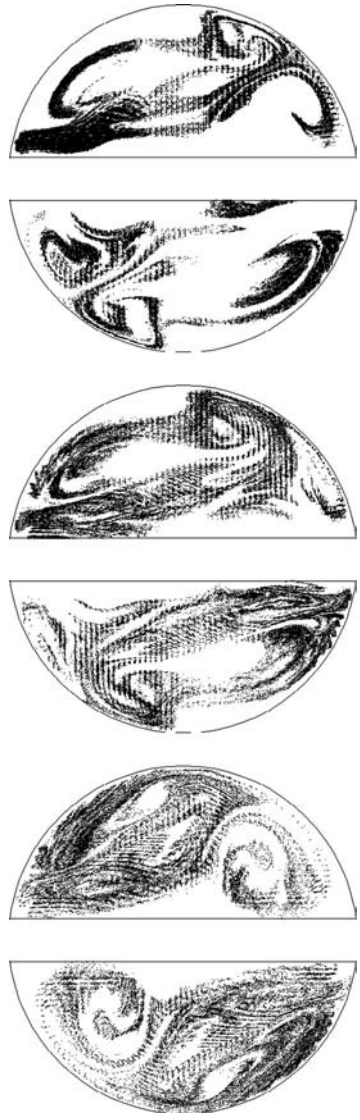

Note: Reproduced from the only available original

Figure 8.
Particles locations at 2nd, 4th, and 6th element

Table VIII.
Structure radius at 2nd, 4th, and 6th mixing element

Mixing element	Structure radius
2nd	0.0408
4th	0.0156
6th	0.0154

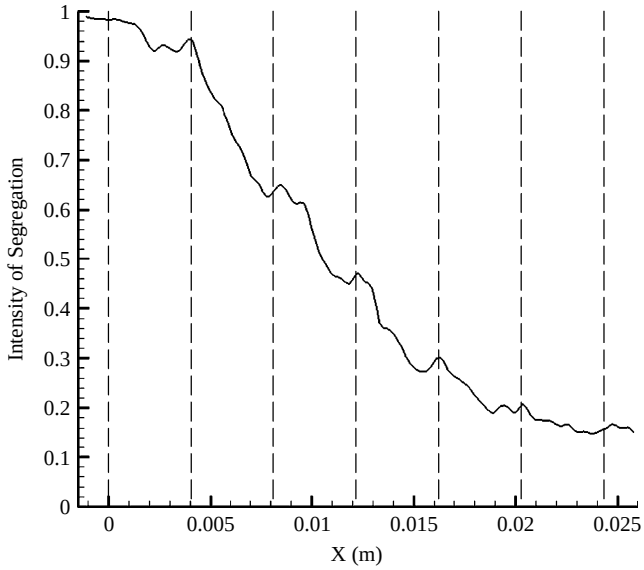

Figure 9.
Intensity of segregation across mixer

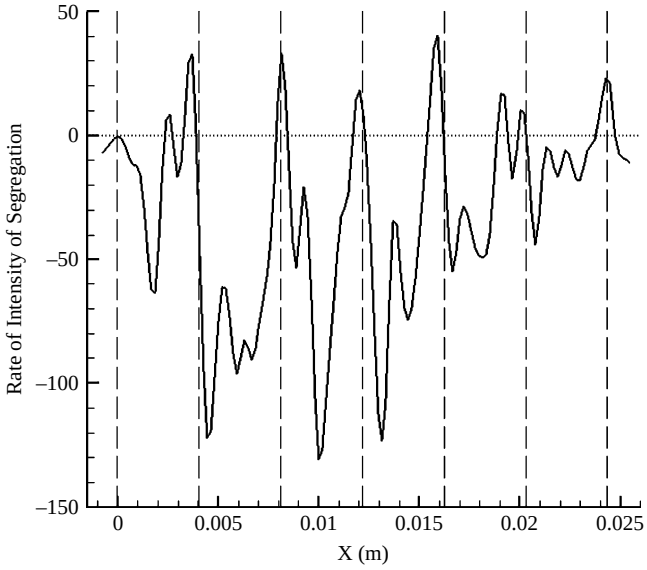

Figure 10.
Rate of intensity of segregation along the axis of mixer

The rate of intensity of segregation changes rapidly in the domain, which is positive in the regions close to the trailing edge of each mixing element and becomes negative as the flow passes the leading edge of each element. This means that helical mixing elements are more effective at their leading edges, suggesting that a compact design with higher length to diameter ratio could help to reach a certain mixing level in a shorter pipe.

The PDU values at different flow cross-sections across the mixer are shown in Figure 11. The PDU value increases as the flow passes through the mixer. As the flow reach the first mixing element, part of the pipe cross-section is filled with the solid material of mixer that leads to a decrease of the PDU value at the leading edge of the first element. The PDU value increases significantly as flow passes the second mixing element and its value continues to increase as the flow passes through the mixer; however, the rate of increase of PDU value decreases when the flow reaches the downstream mixing elements. PDU values follow the same pattern as the values of intensity of segregation. However, the PDU value shows an increase at the end of the first helical mixing element suggesting that the mixing is improving in this region, while intensity of segregation increase in this region suggests the opposite. Considering the distribution of the fluid particles at this region, shown in Figure 7, it is evident that fluid mixing is significantly improved while the flow reaches the trailing edge of the first element.

Conclusion

The performance of a six-element helical static mixer for turbulent flows was studied numerically. The Spalart-Allmaras turbulent mode was shown to be as accurate as the $k - \omega$ model for the study of turbulent flow across a static mixer, while it is computationally less expensive. It was shown that islands of separated fluid elements are distinguishable at the first mixing element. These islands are divided into several small regions after the flow passes the mixing elements. It was observed, that as the flow passes through more mixing elements the distribution of the particles is less affected by the turbulence intensity at the flow inlet. Also, it was seen that the upstream mixing elements increase the mixing more efficiently compared to the downstream mixing elements.

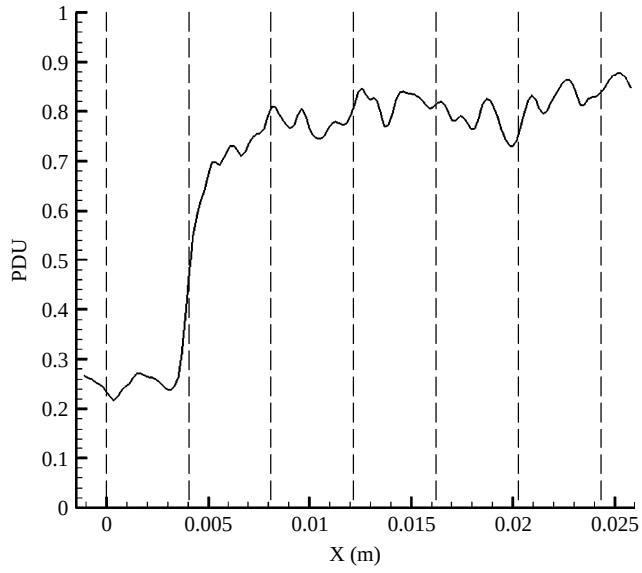

Figure 11.
PDU values across the mixer

References

Baldwin, B.S. and Barth, T.J. (1990), "A one-equation turbulence model for high reynolds number wall-bounded flows", NASA TM 102847.

Byrde, O. (1997), "Massively parallel flow computation with application to fluid mixing", PhD thesis, Ecole Polytechnique Federale de Lausanne, Lausanne.

Byrde, O. and Sawley, M.L. (1999a), "Optimization of a Kenics static mixer for non-creeping flow conditions", *Chemical Engineering Journal*, Vol. 72, pp. 163-9.

Byrde, O. and Sawley, M.L. (1999b), "Parallel computation and analysis of the in a static mixer", *Computers & Fluids*, Vol. 28, pp. 1-18.

Camp, T.R. and Stein, P.C. (1943), "Velocity gradients and internal work in fluid friction", *Journal of The Boston Society of Civil Engineers Section*, Vol. 30 No. 4, pp. 219-37.

Clark, M.M. (1985), "Effect of micromixing on product selectivity", *Proc. AWWA Annual Conference, Denver, CO*, pp. 1957-75.

Dacles-Mariani, J., Zilliac, G.G., Chow, J.S. and Bradshaw, P. (1995), "Numerical/experimental study of a wingtip vortex in the near field", *AIAA Journal*, Vol. 33 No. 9, pp. 1561-8.

Danckwerts, P.V. (1952), "The definition and measurement of some characteristics of mixtures", *Applied Scientific Research*, Vol. A3, pp. 279-96.

Graber, S.D. (1994), "A critical review of the use of the G-value (RMS velocity gradient) in environmental engineering", *Developments in Theoretical and Applied Mechanics*, Vol. 17, pp. 533-56.

Hobbs, D.M. and Muzzio, F.J. (1997), "The Kenics static mixer: a three-dimensional chaotic flow", *Chemical Engineering Journal*, Vol. 67, pp. 153-66.

Hobbs, D.M. and Muzzio, F.J. (1998), "Reynolds number effects on laminar mixing in the kenics static mixer", *Chemical Engineering Journal*, Vol. 70, pp. 93-104.

Jones, S.C. (1999), "Static mixers for water treatment", PhD thesis, Georgia Institute of Technology, Atlanta, GA.

Jones, S.C., Sotiropoulos, F. and Amirtharajah, A. (2002), "Numerical modeling of helical static mixer for water treatment", *Journal of Environmental Engineering*, Vol. 128, pp. 431-40.

Kemblowski, Z. and Pustelnik, P. (1988), "Residence time distribution of a power-law fluid in kenics static mixers", *Chemical Engineering Science*, Vol. 43 No. 3, pp. 473-8.

Khakhar, D.V., Franjione, J.G. and Ottino, J.M. (1987), "A case study of chaotic mixing in deterministic flows: the partitioned-pipe mixer", *Chemical Engineering Science*, Vol. 42, p. 2909.

Kolmogorov, A.N. (1942), "Equations of turbulence motion of incompressible fluid", *Izvestia Academy of Sciences, USSR; Physics*, Vol. 6, pp. 56-8.

Kusch, H.A. and Ottino, J.M. (1992), "Experiments on mixing in continuous chaotic flows", *Journal of Fluid Mechanics*, Vol. 236, p. 319.

Launder, B.E. and Spalding, D.B. (1972), *Mathematical Models of Turbulence*, Academic Press, London.

Lin, F.B. and Sotiropoulos, F. (1997), "Strongly-coupled multigrid method for 3-D incompressible flows using near-wall turbulence closures", *Journal of Fluid Mechanics*, Vol. 119, pp. 314-24.

Menter, F.R. (1994), "Two-equation Eddy-viscosity turbulence models for engineering applications", *AIAA Journal*, Vol. 32 No. 8, pp. 1598-605.

Nauman, E.B. (1991), "On residence time and trajectory calculations in motionless mixers", *The Chemical Engineering Journal*, Vol. 47, pp. 141-8.

Nürnberger, D. and Greza, H. (2002), "Numerical investigation of unsteady transitional flows in turbomachinery components based on a RANS approach", *Flow, Turbulence and Combustion*, Vol. 69, pp. 331-53.

Onwulata, C. (2005), *Encapsulated and Powdered Foods*, Taylor & Francis, CRC Press, Boca Raton, FL.

Prandtl, L. (1945), "Über ein neues Formelsystem für die ausgebildete Turbulenz", pp. 6-19, Narc. Akad. Wiss. Göttingen, *Math-Phys. Kl.*

Rahmani, R.K., Keith, T.G. and Ayasoufi, A. (2005), "Three-dimensional numerical simulation and performance study of an industrial helical static mixer", *ASME Journal of Fluids Engineering*, Vol. 127 No. 3, pp. 467-83.

Rahmani, R.K., Keith, T.G. and Ayasoufi, A. (2006a), "Numerical study of the heat transfer rate in a helical static mixer", *ASME Journal of Heat Transfer*, Vol. 128 No. 8, pp. 769-83.

Rahmani, R.K., Keith, T.G. and Ayasoufi, A. (2006b), "Numerical simulation and mixing study of pseudo-plastic fluids in an industrial helical static mixer", *ASME Journal of Fluids Engineering*, Vol. 128 No. 3, pp. 467-80.

Rahmani, R.K., Ayasoufi, A. and Keith, T.G. (2006c), "A numerical study of the global performance of two static mixers", *ASME Journal of Fluids Engineering*, Vol. 129 No. 3, pp. 338-49.

Sotiropoulos, F. and Ventikos, Y. (1998), "Flow through a curved duct using nonlinear two-equation turbulence model", *AIAA Journal*, Vol. 36, pp. 1256-62.

Spalart, P. and Allmaras, S. (1992), "A one-equation turbulence model for aerodynamic flows", Technical Report AIAA-92-0439, American Institute of Aeronautics and Astronautics, Reston, VA.

Tung, T.T. (1976), *Low Reynolds Number Entrance Flows: A Study of a Motionless Mixer*, PhD thesis, University of Massachusetts, Amherst, MA.

Vandoormaal, J.P. and Raithby, G.D. (1984), "Enhancements of the SIMPLE method for predicting incompressible fluid flows", *Numerical Heat Transfer*, Vol. 7, pp. 147-63.

Warming, R.F. and Beam, R.M. (1975), "Upwind second-order difference schemes and applications in unsteady aerodynamic flows", *Proc. AIAA 2nd computational fluid dynamics conference, Hartford, CT*, pp. 17-28.

Wilcox, D.C. (1988), "Reassessment of the scale-determining equation for advanced turbulence models", *AIAA Journal*, Vol. 26 No. 11, pp. 1299-310.

Corresponding author
Ramin K. Rahmani can be contacted at: rkhrahmani@yahoo.com